Sentinel-1 sar observations of peak wavelength and dominant wave direction in the marginal ice zone of the barents sea

Monteban, D.; Lubbad, R.; Johnsen, H.

Published in:
Proceedings of the International Conference on Port and Ocean Engineering under Arctic Conditions (POAC)

Publication date:
2019

Document Version
Publisher's PDF, also known as Version of record

Proceedings of the 25th International Conference on
Port and Ocean Engineering under Arctic Conditions
June 9-13, 2019, Delft, The Netherlands

Sentinel-1 SAR observations of peak wavelength and dominant wave direction in the marginal ice zone of the Barents Sea

Dennis Monteban[1,2], Raed Lubbad[2], Harald Johnsen[3]
[1] DTU Space, Technical University of Denmark, Lyngby, Denmark
[2] The Norwegian University of Science and Technology (NTNU), Trondheim, Norway
[3] Norut (Northern research Institute), Tromsø, Norway

ABSTRACT

Synthetic aperture radar (SAR) has proven to be a very important source of data in the Polar regions because it covers large areas continuously, independent of the weather and time of day. In this study, we make use of Sentinel-1 Interferometric wide (IW) swath SAR images to study the change in peak wavelength and dominant wave direction of long waves traveling through icy waters in the Barents Sea. We verify our estimates of the open water peak wavelength and dominant wave direction by comparing the results from the Sentinel-1 SAR with in-situ buoy measurements, which are part of the *Barents Sea Metocean and Ice Network* (BaSMIN) measurement campaign.

We find that the peak wavelength increases as waves propagate into the sea ice. This agrees well with our knowledge of wave penetration into the MIZ, where the sea ice acts as a natural low pass filter on the ocean waves. A consequence of this is the disappearance of the high frequency waves from SAR images over the sea ice especially at a distance from the ice edge. Since the presence of high frequency waves blur the SAR images, SAR images in sea ice become of higher quality compared to images over the open ocean. As a result, the spread in observations of the peak wavelength is much larger in the open water than within the sea ice.

Further, the dominant wave direction changes towards the normal, relative to the ice edge. This can be motivated by Snell's law and agrees with findings from previous studies. A large shift of the dominant wave direction is found in the vicinity of the ice edge, which is partly physical due to wave refraction and is partly an imaging artefact. The latter stems from that fact that the azimuth cut-off (i.e., loss of spatial resolution along track) is much smaller in the sea ice than in open water and thus waves that were not visible in images over the open water may appear in images over the sea ice. This causes an apparent shift in wave direction close to the ice edge that is purely due to SAR imaging. We demonstrate this effect with our processed images.

KEY WORDS: SAR; Sentinel-1, Marginal Ice Zone, Ocean waves, Sea ice; BaSMIN measurement programme

Introduction

Due to climate change, the Polar regions are experiencing dramatic sea ice reductions. The reduced sea ice cover gives rise to longer open water seasons and will lead to increased commercial activities in the Arctic. For safety reasons it is extremely important to forecast the wave-climate. However, to accurately predict the wave climate in ice-covered oceans, we need to have a proper understanding of the interactions between ocean waves and sea ice.

Sea ice can be classified based on its position to land as: landfast ice zone, shear zone and the marginal ice zone (MIZ). The MIZ is closest to the open water and depending on time and location, a continuous ice sheet, floe aggregates, pancake ice, brash ice and grease ice can be found in this zone (e.g., Zhao et al., 2015). Further, it is the most dynamic and complex zone, as the sea ice is affected by ocean waves through for instance ice breakup (Kohout et al., 2016) ice drift (Perrie and Hu, 1997) and rafting (Dai et al., 2004). Not only do waves affect the sea ice cover, but also the ice has a strong impact on the waves, making the study of wave-ice interactions a two-way coupled problem. Waves propagating through ice-covered oceans show a reduction in amplitude due to wave scattering and dissipation (e.g., Squire 2018). Scattering redistributes the energy and is a conservative process, i.e., no energy is lost. Dissipation on the other hand removes energy from the waves. The ice also affects the waves by refraction, reflection and it changes the dispersion relation (e.g., Squire et al., 1995).

The propagation of ocean waves into the MIZ has been studied by remote sensing for a few decades. Especially synthetic aperture radar (SAR) satellite images are capable of wave measurements in icy waters. In this study, we make use of Sentinel-1 SAR imagery and focus on the change in peak wavelength and dominant wave direction for waves propagating within sea ice in the Barents Sea.

SAR observations have been used to study ocean waves within sea ice, see the review by Monteban et al. (2019). These observations have proven to be a valuable source of information because SAR can operate day and night, independent of the weather, and it can cover a vast area at once. One of the mechanisms that allow the imaging of ocean waves by SAR is velocity bunching (e.g., Alpers et al., 1981). The velocity bunching of short waves blurs the image and results in the well-known azimuth cut-off effect (e.g., Kerbaol et al., 1998). This effect becomes much smaller in sea ice, because the ice cover acts as a low pass filter on the waves and the short wavelengths of wind driven sea are the dominant contribution to the azimuth cut-off. The difference in azimuth cut-off wavelength causes an apparent shift in dominant wave direction close to the ice edge. This happens when comparing an image over open water (with a high azimuth cut-off) with its adjacent image over the sea ice (with a lower azimuth cut-off). Thus, the anticipated change in dominant wave direction from SAR images when waves enter the sea ice is not entirely based on physical processes, but part of it is an imaging effect (Schulz-stellenfleth and Lehner, 2002). A good example of this is given in (Stopa et al., 2018), their Figure 1d, where a significant change in wave direction between an open water area and an ice-covered area can be seen.

The first detailed study on wave refraction at the ice edge was done by Liu et al. (1991), using aircraft SAR. They argued that the critical angle which determines if waves are reflected or refracted, can be found by Snell's law and they showed that it was in agreement with the SAR observations. Shen et al. (2018) studied long waves propagating from the open water into the MIZ with the RADARSAT-2 SAR satellite at the East side of Greenland. They found a lengthening of the peak wavelength in the MIZ and a change in dominant wave direction. Moreover, they reported that the dominant wave direction changes towards the normal direction, relative to the ice edge. The same storm system as studied by Shen et al. (2018) was studied by Gebhardt et al. (2016) using the TerraSAR-X satellite. The TerraSAR-X satellite

orbits at an altitude of ~500 km, which is lower than the Sentinel-1 (~700 km) and RADARSAT-2 (~800 km). The low altitude of the TerraSAR-X satellite is advantageous against the non-linear imaging effects of ocean waves (Gebhardt et al., 2015), and has for instance a smaller azimuth cut-off. Gebhardt et al. (2016) looked at the change in peak wavelength for waves travelling long distances (in the order of 1000 km). They found that the observed wavelengths from the TerraSAR-X images are consistent with the spatial dispersion of waves on the open water. The largest increase of the peak wavelength was found in the MIZ, which is most likely due to wave-ice interactions. The study of Stopa et al. (2018) reported, amongst others, the change in wave direction when waves enter the sea ice in the Beaufort Sea. A change of 20-30° is found at the ice edge and further into the ice pack another large change in wave direction is observed. The authors expect that the large change in wave direction is due to refraction, either at the ice edge or due to a change in ice thickness.

In this study we make use of Sentinel-1 SAR imagery and focus on the change in peak wavelength and dominant wave direction when waves propagate within the sea ice. The peak wavelength and dominant wave direction are in this study inferred from the wavenumber and direction associated with the maxima of the image cross spectrum as will be shown later. We study a wave event with long waves captured by the Sentinel-1A satellite, which took place on the 4th of April 2017 in the Barents Sea. We present also new in situ data, which are part of the *Barents Sea Metocean and Ice network* (BaSMIN) measurement campaign. This in situ data are used to verify our derived peak wavelength and dominant wave direction from Sentinel-1 in the open water. The measurement campaign and the studied wave event are introduced in the next section. The wave parameters are derived from the real part of the cross spectrum directly, without applying a modulation transfer function. The cross spectrum is derived using the method of Johnsen & Collard (2009) and the main parts are described in this paper. The obtained peak wavelength and dominant wave direction show an increased peak wavelength and a wave direction change towards the normal as waves penetrate the MIZ.

BaSMIN measurement programme

The BaSMIN field campaign took place from October 2015 until October 2018. This campaign was undertaken by Fugro GEOS Ltd on behalf of Equinor (former Statoil). Five wave scan moorings and five ice profiling moorings were deployed. The wave scan moorings measured current speed and direction, seawater temperature, salinity, wave parameters, atmospheric pressure and temperature, and relative humidity. The ice profile moorings measured ice draft, ice velocity, current velocity, sea water temperature, salinity and pressure. The measurement locations are shown in Figure 1. The relevant in situ data for this project are the wave data collected at wave scan mooring three (WS3). The wave rose and the relation between significant wave height and mean wave period are presented in Figure 2. The dominant direction where the waves come from is west-southwest. Moreover, the highest and longest waves are coming from this direction. This is to be expected, as this is the directional sector which has the largest wave generating fetch.

We studied a wave event that occurred on the 4th of April 2017. This event is characterized by long waves, with a significant wave height of roughly 5 meters and a peak wavelength of 163 meter, measured at wave buoy WS3. The waves propagate approximately from east to west. Sentinel-3 altimetry and Sentinel-1 SAR data were collected during this event. In Figure 1, a Sentinel-3 altimetry track provides the significant wave height and matches the observations at the wave scan moorings well (not shown here). Further, a Sentinel-1 Extra-Wide swath (EW) image is provided. The brighter regions indicate the ice and the darker regions the open water. From this image the approximate location of the ice edge can be seen, and all the ice mooring stations are circumpassed by the sea ice. During this wave event, the ice draft measured at the five ice moorings are in the range of 0.2 – 0.4 m and the ice is therefore thin ice.

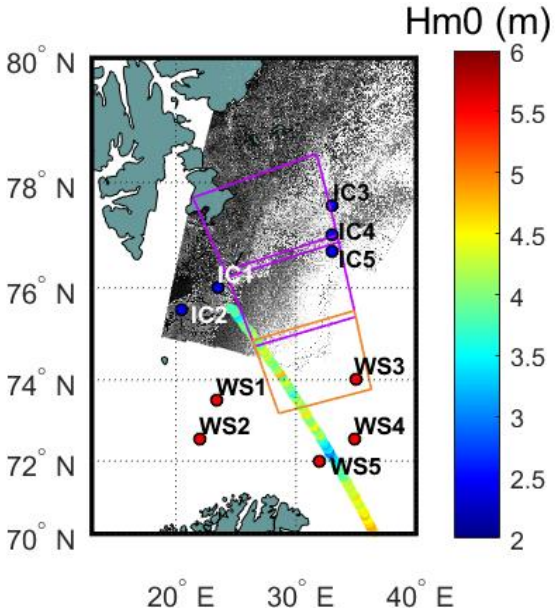

Figure 2. Overview of the BaSMIN measurement locations in the Barents Sea. The red dots indicate the wavescan moorings (WS) and the blue dots the ice mooring locations (IC). A Sentinel-1 EW image is plotted in gray scale, where the lighter areas indicate sea ice. Further, a Sentinel-3 altimetry track is overlaid with the significant wave height (Hm0) given in colour code. The purple and orange rectangles show the extent of Sentinel-1 IW images used to derive the peak wavelength and dominant wave direction. All the satellite data is acquired on the 4th of April 2017.

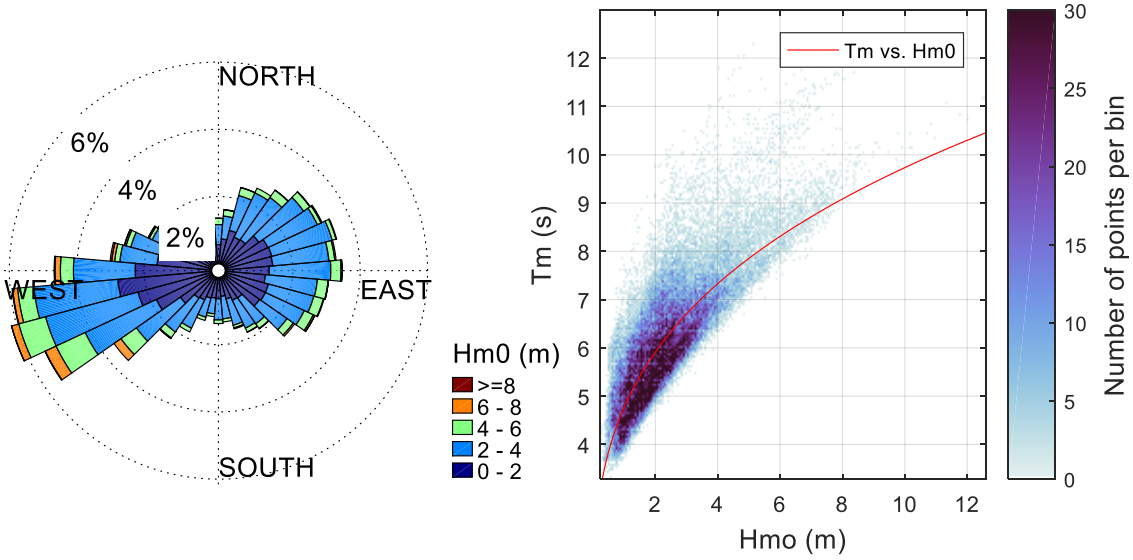

Figure 1. Left figure presents a wave rose and shows the direction from where the waves come from. The right figure shows a scatter plot of the significant wave height (Hm0) vs mean wave period (Tm). The red line is a fit through the data. Both figures show data from wavescan location 3 (WS3) for the entire period of the BaSMIN measurement campaign.

Sentinel-1 data and processing

In this study, we used data collected by ESA's Sentinel-1A satellite. The Sentinel-1 constellation consists of two polar orbiting satellites, carrying a C-band SAR instrument with a frequency of 5.4 GHz. The instrument supports both single and dual polarization. Further, it can operate in four different acquisitions modes that include Stripmap (SM), Interferometric Wide swath (IW), Extra-Wide swath (EW) and Wave (WV). The incidence angle varies between 30° and 46°. We used data collected on the 4th of April 2017, acquired in the IW

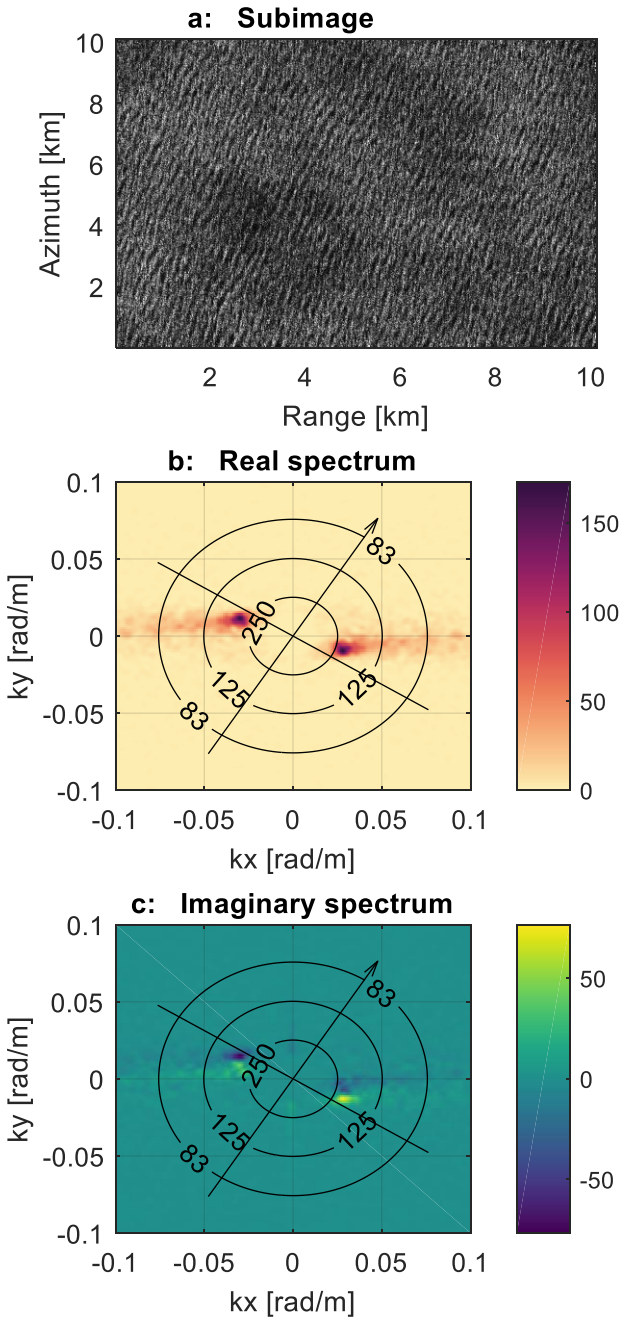

Figure 3. (a) Typical fragment of the Sentinel-1 IW radar scene acquired on the 4th of April 2017, used for the calculation of the cross spectrum. The cross spectrum consists of a real part (panel b) and an imaginary part (panel c). k_x is the wavenumber in range direction and k_y is the wavenumber in azimuth. The arrow points towards north and the overlaid circles indicate the wavelength.

acquisition mode and both HH and HV polarization were available. Throughout this study, we used the HH polarization. The data are a level-1 Single Look Complex (SLC) product that can freely be downloaded from ESA's Sentinel Data Hub. For this data product, the phase information is preserved. This phase information allows us to produce multi looks from which the cross spectrum is calculated (Engen and Johnsen, 1995). The resolution of the data is approximately 3.5 by 14 meter, in range (perpendicular to flight path) and azimuth (along the flight path), respectively. The extent of the data acquired can be seen in Figure 1, indicated by the purple and orange rectangles. Each rectangle is the extent of one data product.

To calculate the peak wavelength and dominant wave direction, we use images of roughly 10 x 10 km. An example is given in Figure 3a, where the normalized intensity is plotted. This complex subimage is first processed into three different sub looks and the cross spectrum is computed between them, following the method of Johnsen & Collard (2009). The resulting real part and imaginary part of the cross spectrum computed from the image in Figure 3a are given in Figure 3b and Figure 3c, respectively. Waves longer than 300 meters are removed from the spectrum by masking out the centre.

From the real part of the cross spectrum, we can find the peak wavelength and the dominant wave direction from the direction and wavenumber of the maximum of the spectrum, but only to within a sign. This is referred to as the 180° wave ambiguity, i.e., it is not clear if the waves come from approximately east or west in this example. This had been a fundamental difficulty in SAR imaging, because traditional SAR images did not include phase information and thus provided a snapshot of the sea surface. With the applied cross-spectral method here, originally developed by Engen & Johnsen (1995), we can solve the 180° wave ambiguity problem. The obtained imaginary part of the cross spectrum has a positive and a negative peak. When the peak in the real part of the cross spectrum matches the positive peak in the imaginary part, this is where the waves are coming from (e.g., Bao & Alpers 1998). Therefore, for the example given in Figure 3, the waves propagate from almost east to west.

The obtained real part of the cross spectrum, also called the image intensity spectrum, is connected to the ocean wave spectra by a Modulation Transfer Function (MTF). This relation is expressed as (e.g., Hasselmann et al., 1985):

$$P(k) = S(k) * R^{SAR}(k)^{\,2} \tag{1}$$

where $P(k)$ and $S(k)$ are the image intensity spectrum and the ocean wave spectrum, respectively, and $R^{SAR}(k)$ is the MTF. The MTF is a combination of tilt and hydrodynamic modulation in addition to velocity bunching (e.g., Alpers et al., 1981). The MTF has in general a limited effect on the derived peak wavelength and wave direction (e.g., Gebhardt et al., 2016) for range traveling waves and for long waves, not affected by the azimuth cut-off. For our studied wave event, the waves travel near range and are relatively long waves. Therefore, we directly obtain these wave parameters from the image intensity spectrum and do not use an MTF.

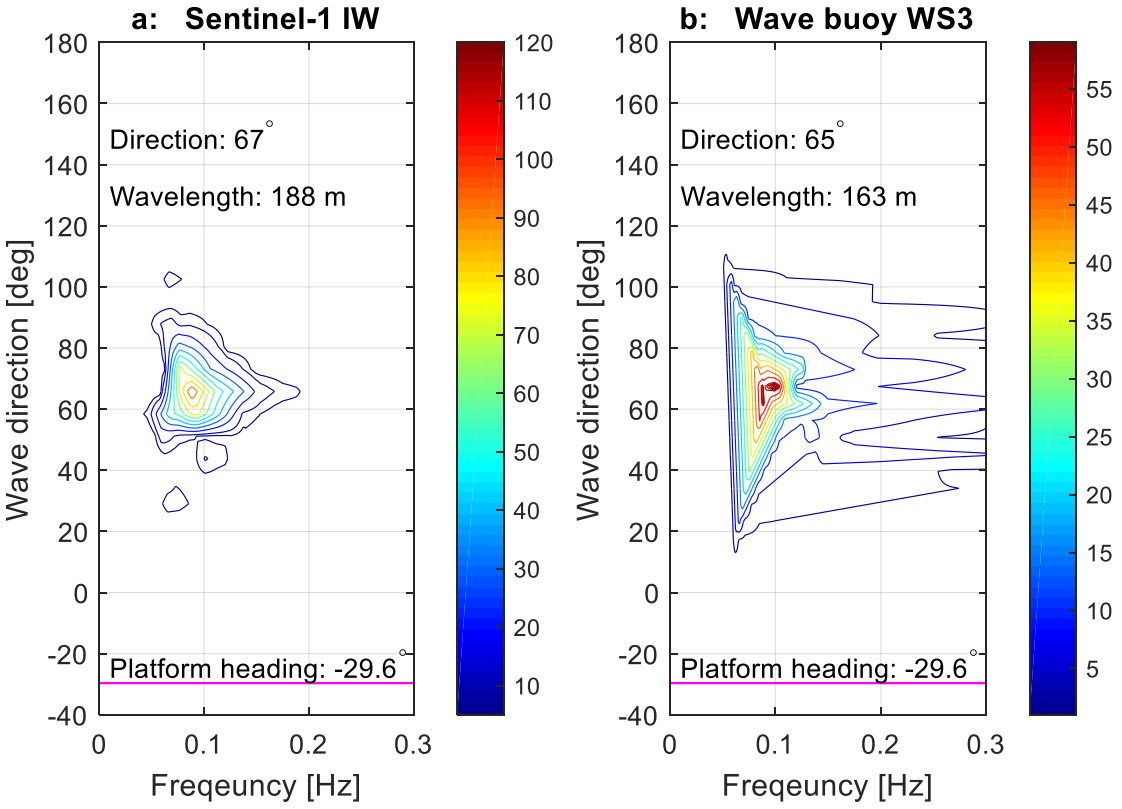

Figure 4. (a) The intensity image spectrum as computed from the Sentinel-1 IW subimage of 10 x 10 km over wave scan mooring WS3. The 180° ambiguity has already been removed and the wave direction indicates the direction the waves are coming from, with respect to north (0° on the y-axis). The frequency spectrum given in panel (a) is calculated from the wavenumber spectrum and using the open water dispersion relation. In addition, the platform heading is shown with the magenta line and indicates the range direction. (b) The wave spectrum obtained at wave buoy WS3. Note that the two plotted spectra are fundamentally different and cannot be directly compared. The relation between the two spectra is given in Eq. (1).

Results

In this section, we present the results of the processed Sentinel-1 IW imagery obtained on the 4th of April 2017. First, we verify our obtained wave parameters in the open ocean with measurements from wave buoy WS3. Then we present the estimated peak wavelength and dominant wave direction in the open water and within the ice-covered ocean. Finally, we demonstrate the azimuth cut-off effect by studying a wave system traveling in azimuth direction and entering the sea ice.

Comparison of the peak wavelength and dominant wave direction with wave buoy WS3

A subimage of the radar scene of roughly 10 x 10 km over buoy WS3 (extent of radar scene is shown with an orange rectangle in Figure 1) is processed and the derived peak wavelength and dominant wave direction are compared with in-situ data from buoy WS3. The image intensity spectrum as obtained from Sentinel-1 and the ocean wave spectrum acquired by wave buoy WS3 are shown in Figure 4. For a one-to-one comparison of the two spectra, one would have to convert the intensity image spectrum from the Sentinel-1 imagery to the wave spectrum using Eq. (1). However, we are only interested in the peak wavelength and dominant wave direction, so we did not do this conversion. The obtained values of the peak wavelength and dominant wave direction from the Sentinel-1 image are 188 m and 67°, respectively. This is satisfactory when compared with the measured wavelength of 163 m and dominant wave direction of 65° from the wave buoy.

Peak wavelength and dominant wave direction

The peak wavelength and dominant wave direction are estimated on subimages of 10 x 10 km, both in the open water and in the sea ice. This is done for two Sentinel-1 IW data products; the extent is shown with the purple rectangles given in Figure 1. The derived wave parameters are plotted in Figure 6 on top of the Sentinel-1 IW images. Each arrow is the average of four different subimages, so it represents an area of roughly 20 x 20 km. The direction of the arrows is very consistent over the range direction. Moreover, the waves are travelling in the open water almost in range direction. This corresponds to waves travelling from east-northeast. The wave direction clearly changes upon entering the sea ice. To better demonstrate the change, we plotted the dominant wave direction in the azimuth direction for fixed range locations in Figure 5b. In addition, the change in dominant wave direction over azimuth, averaged over range, is also plotted in the same figure. We see that the waves come from roughly 70°, with respect to north, in the open water. At the location of the ice edge we see a large shift in direction of roughly 30°. In the sea ice we see a gradual change in wave direction and over approximately 220 km the waves show a directional change of roughly 22°.

The colour of the arrows in Figure 6 indicates the peak wavelength. The derived peak wavelength shows quite some variation over the range direction and it is hard to see the change for waves entering the sea ice from this figure directly. In Figure 5a, the change of the peak wavelength in the azimuth direction is plotted for subimages with a fixed range position. Two things are evident from this figure. The first is that the spread in the estimated peak wavelength is much larger in the open water than within the sea ice. Second, the change of the peak wavelength in azimuth, when averaged over range direction, clearly shows an increase in peak wavelength from the ice edge to roughly 220 km into the ice pack. The peak wavelength for waves that just entered the ice is 210 m, while the peak wavelength 220 km into the sea ice is roughly 231 m.

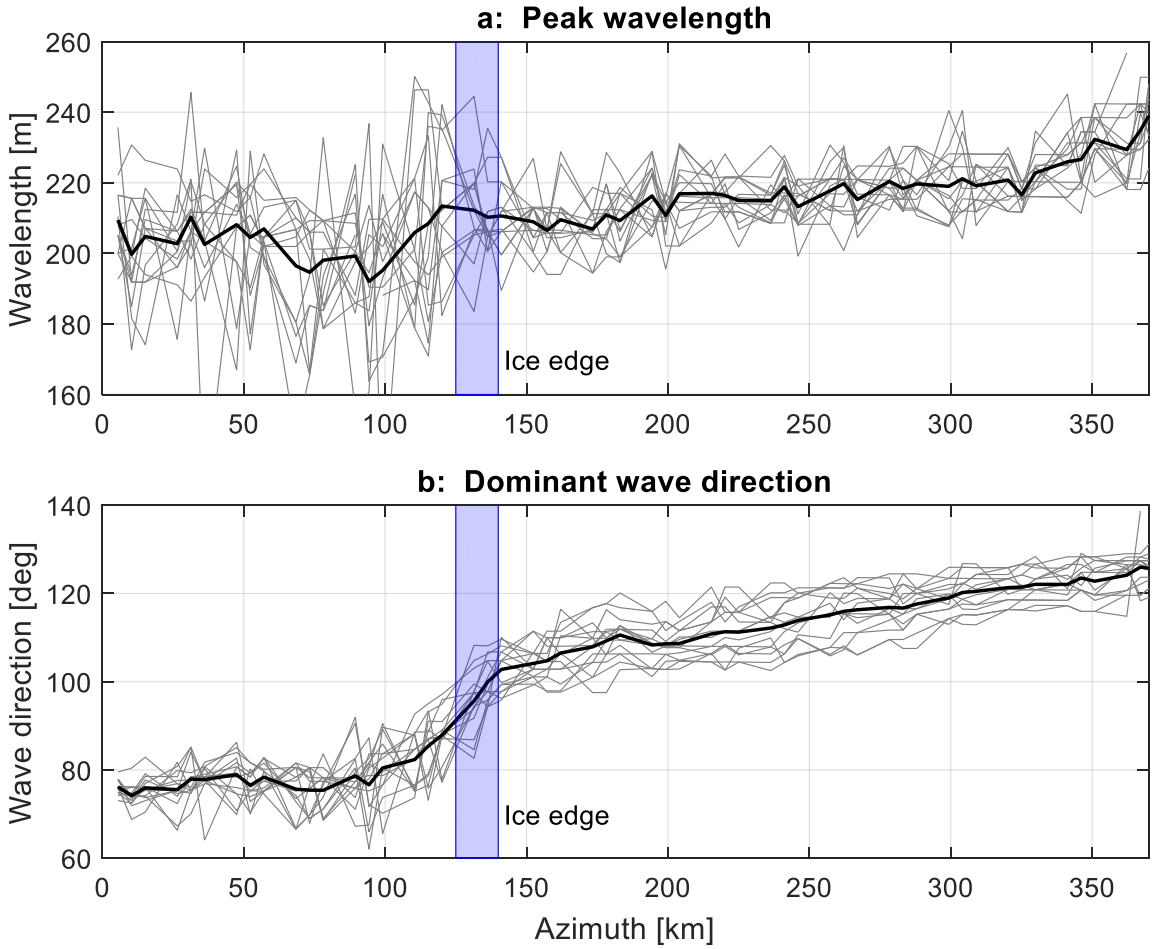

Figure 5. The top figure (a) shows the peak wavelength and the bottom figure (b) displays the dominant wave direction, derived from subimages of 10 x 10 km. The light gray lines show the result of all the subimages in azimuth direction, for a fixed range coordinate. The range positions are 10 km apart. The solid black line shows the results averaged over range direction, i.e., the mean of the light gray lines. The start of ice edge is indicated with the coloured area and is estimated from Figure 6.

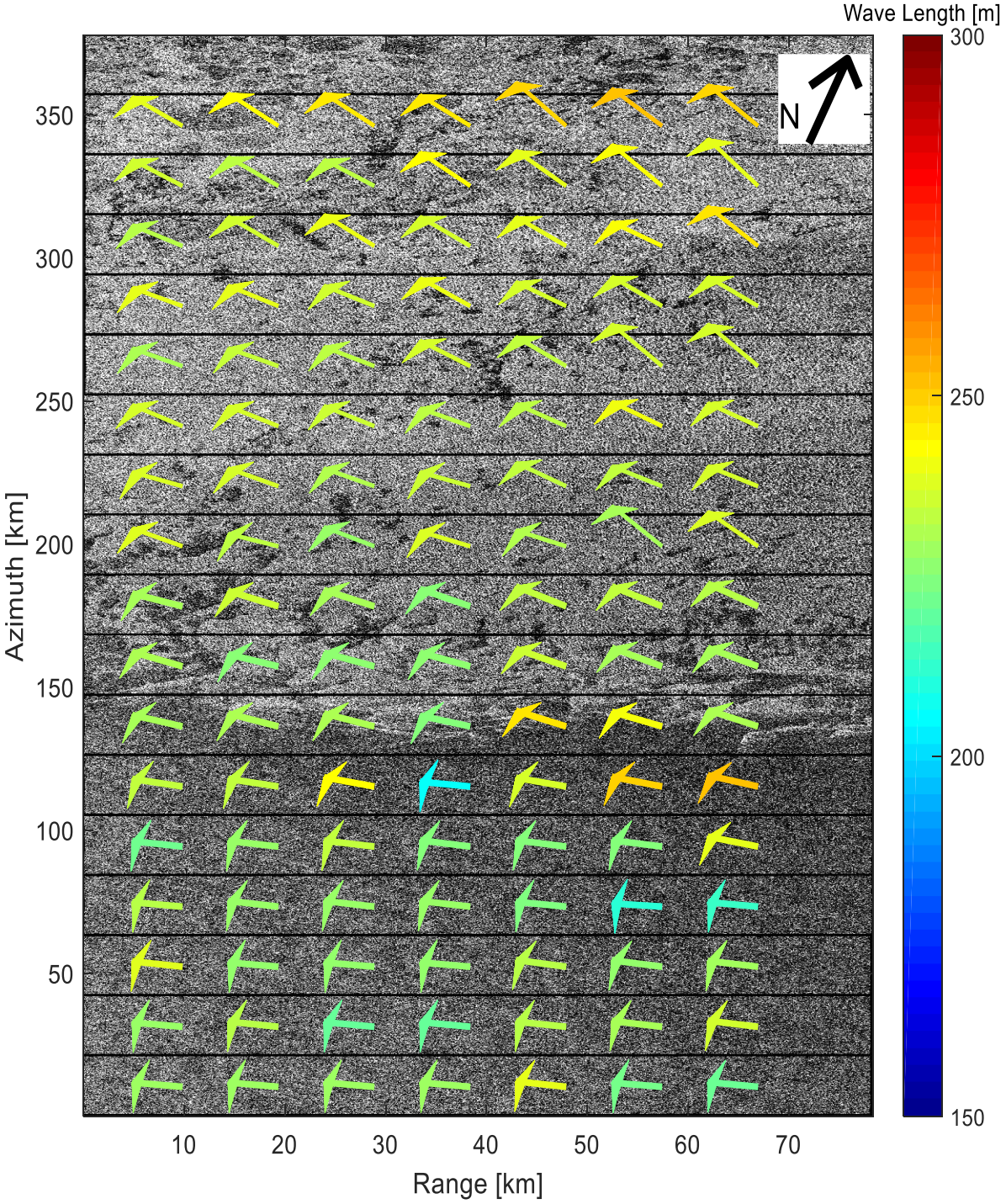

Figure 6. Sentinel-1 IW normalized intensity map (gray scale). The extent is shown in Figure 2 with the two purple rectangles. The brighter regions indicate sea ice, while the darker regions are open water. The ice edge starts around 130-140 km in azimuth direction. The overlaid arrows show the derived peak wavelength and dominant wave direction for subimages of approximately 20 x 20 km. The arrows point in the direction the waves are moving towards and the colour indicates the peak wavelength.

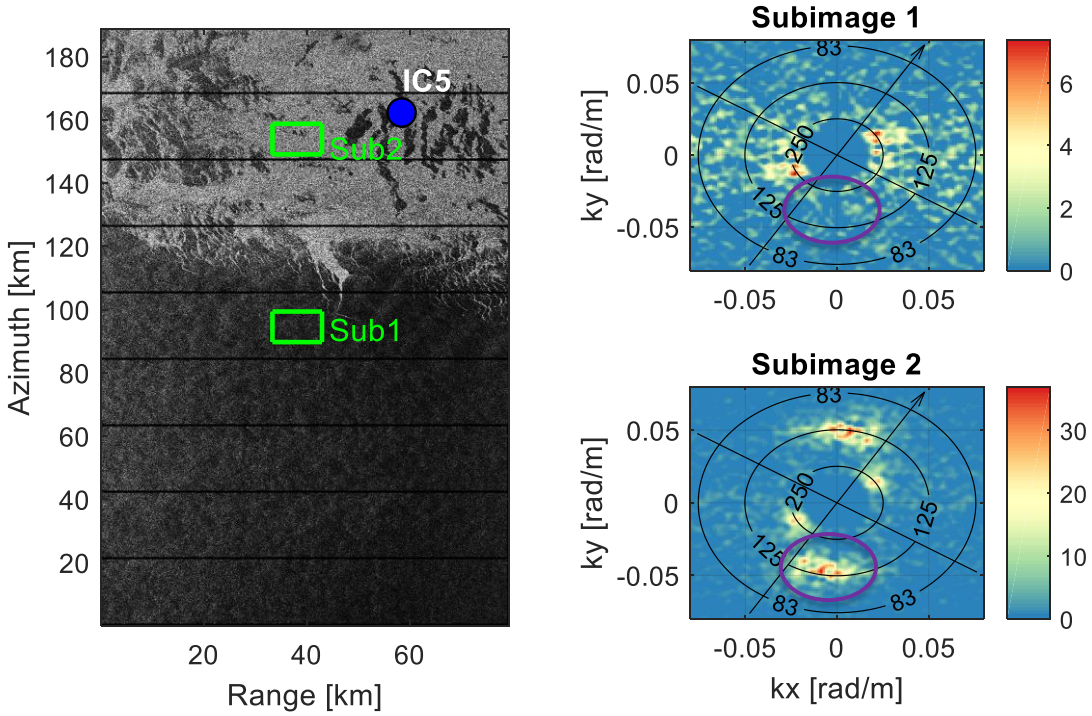

Figure 7. Illustration of the azimuth cut-off effect. The left figure shows a normalised intensity map (gray scale), acquired by Sentinel-1 IW on the 22nd of April 2017. The two image intensity spectra plotted on the right are calculated from the two subimages indicated by the green squares. Note that the 180° wave ambiguity is not removed from the spectra. k_x is the wavenumber in range direction and k_y is the wavenumber in azimuth. The arrow points towards north and the overlaid circles indicate the wavelength.

Azimuth cut-off: open water versus sea ice

The azimuth cut-off effect can nicely be demonstrated when comparing SAR imagery over the open ocean compared to imagery over the sea ice. This is demonstrated in Figure 7. A wave event was captured on the 22nd of April 2017, where two wave systems are present. One swell system traveling close to the range direction and another swell system traveling in the azimuth direction. The image intensity spectra are computed for a subimage over the open ocean (subimage 1) and over the sea ice (subimage 2). The swell system traveling in azimuth direction is not visible in the open ocean but does appear in the sea ice (compare the area in the purple ovals). This is because the azimuth cut-off wavelength is much smaller in the sea ice compared to the open ocean.

Discussion and Conclusions

In this paper we have demonstrated the change in peak wavelength and dominant wave direction of long waves entering the MIZ in the Barents Sea. We used Sentinel-1 SAR imagery, acquired on the 4th of April 2017. The peak wavelength and dominant wave direction are directly inferred from the direction and wavenumber associated with the maxima of the image intensity spectrum, i.e., from the real part of the image cross spectrum. This approach to directly infer the peak wavelength and dominant wave direction from the image spectrum, without applying an MTF, was also applied by Gebhardt et al. (2016) on TerraSAR-X imagery. This approach implies an assumption of a linear relationship between the image intensity spectrum and wave spectrum (Gebhardt et al., 2015) and was validated by Bruck & Lehner (2012) using the TerraSAR-X satellite. This relationship holds for waves traveling near range, or for very long waves that are not affected by the azimuth cut-off. Further, when there is a linear relationship, the maximum value of the image intensity spectrum is not significantly altered by the MTF. For our studied wave event, the waves travel near range and are long waves, suggesting a linear relationship. We verified our derived peak wavelength and dominant wave

direction from Sentinel-1 with buoy measurements. The derived values are in good agreement with the measurements, giving confidence in the obtained values for the studied wave event.

The derived peak wavelengths show an increase as the waves enter the MIZ. At the ice edge the peak wavelength is roughly 210 m, while further into the ice pack it is increased to 231 m. This increase in peak wavelength agrees with our understanding of wave penetration into the MIZ. The sea ice found in the MIZ scatters and dissipates the high frequency ocean waves, thereby acting as a low pass filter (Collins et al., 2015). However, part of the increase in peak wavelength can be attributed to the spatial dispersion of waves in the open water (e.g., Gebhardt et al. (2016). Furthermore, the spread in derived peak wavelength in the open water is much larger than for sea ice, see Figure 5a. This can be attributed to the fact that the high frequency waves are not present in the sea ice. The random motions of the short waves blur the image (Alpers and Rufenach, 1979) and the absence of short waves enhances wave visibility in the sea ice (Lyzenga et al., 1985). Therefore, the derived values of the peak wavelength show less spread in the sea ice as the quality of the image is better than in the open ocean.

The dominant direction of the waves coming from the open ocean is roughly 70°, with respect to north. Upon entering the sea ice, a large shift in wave direction of roughly 30° is found. Further in the sea ice the change is small and gradual. The change in dominant wave direction at the ice edge is the largest and in the earliest studies with SAR (e.g., Liu et al., 1991; Shuchman et al., 1994), this change was solely attributed to refraction. However, due to the damping of short waves by the ice, the azimuth cut-off is much smaller in the sea ice compared to the open ocean, as is nicely demonstrated in Figure 7, where waves that are not visible in the open ocean do appear in the image over the sea ice. Therefore, part of the change in dominant wave direction is an imaging artefact, as was demonstrated by Schulz-stellenfleth & Lehner (2002). The result is that the large shift of 30° at the ice edge is partly an imaging artefact and can partly be attributed to refraction. The azimuth cut-off is largest for waves traveling in azimuth direction and it disappears for waves traveling in range direction (e.g., Alpers et al., 1981). Because the waves travel almost in range direction in the open water, we expect that the large change in dominant wave direction at the ice edge is mainly due to refraction. Further, the change in dominant wave direction is towards the normal, relative to the ice edge. This can be motivated by Snell's law, which is in agreement with the results of Liu et al. (1991). This change in wave direction results in wave convergence when the ice edge has a circular shape, potentially leading to a region of increased wave energy and may contribute to ice break up (Shen et al., 2018).

The observations provided in this paper can be used to validate theoretical models such as the viscous layer model or the scattering model, as was for instance done in the study of Shen et al. (2018). Furthermore, the results once again show the great potential of SAR. The availability of freely downloadable data from ESA's Sentinel missions will most certainly improve the understanding of the complex interactions between ocean waves and sea ice.

Acknowledgements

We would like to thank and acknowledge Equinor (former Statoil) and the other BaSMIN JIP members for kindly making the data recorded in the Barents Sea available for this study. The Sentinel-1 and Sentinel-3 data are provided by the European Space Agency (ESA) and can freely be downloaded from ESA's Sentinel data hub. Further we would like to acknowledge the support from the SAMCoT CRI through the Research Council of Norway and all the SAMCoT partners.

References

Alpers, W., Rufenach, C., 1979. The effect of orbital motions on synthetic aperture radar imagery of ocean waves. IEEE Trans. Antennas Propag. 27, 685–690. https://doi.org/10.1109/TAP.1979.1142163

Alpers, W.R., Ross, D.B., Rufenach, C.L., 1981. On the detectability of ocean surface waves by real and synthetic aperture radar. J. Geophys. Res. Ocean. 86, 6481–6498. https://doi.org/10.1029/JC086iC07p06481

Bao, M., Alpers, W., 1998. On the cross spectrum between individual-look synthetic aperture radar images of ocean waves. IEEE Trans. Geosci. Remote Sens. 36, 922–932. https://doi.org/10.1109/36.673683

Bruck, M., Lehner, S., 2012. Sea state measurements using TerraSAR-X data. Geosci. Remote Sens. Symp. (IGARSS), 2012 IEEE Int. 7609–7612. https://doi.org/10.1109/IGARSS.2012.6351866

Collins, C.O., Rogers, W.E., Marchenko, A., Babanin, A. V, 2015. in the Arctic marginal ice zone. Geophys. Res. Lett. 42, 1863–1870. https://doi.org/10.1002/2015GL063063.Received

Dai, M., Shen, H.H., Hopkins, M.A., Ackley, S.F., 2004. Wave rafting and the equilibrium pancake ice cover thickness. J. Geophys. Res. C Ocean. 109, 1–9. https://doi.org/10.1029/2003JC002192

Engen, G., Johnsen, H., 1995. SAR-Ocean Wave Inversion Using Image Cross Spectra. IEEE Trans. Geosci. Remote Sens. 33, 1047–1056. https://doi.org/10.1109/36.406690

Gebhardt, C., Bidlot, J.R., Gemmrich, J., Lehner, S., Pleskachevsky, A., Rosenthal, W., 2016. Wave observation in the marginal ice zone with the TerraSAR-X satellite. Ocean Dyn. 66, 839–852. https://doi.org/10.1007/s10236-016-0957-8

Gebhardt, C., Pleskachevsky, A., Rosenthal, W., Lehner, S., Hoffmann, P., Kieser, J., Bruns, T., 2015. Comparing wavelengths simulated by the coastal wave model CWAM and TerraSAR-X satellite data. Ocean Model. 103, 133–144. https://doi.org/10.1016/j.ocemod.2015.10.003

Hasselmann, K., Raney, R.K., Plant, W.J., Alpers, W., Shuchman, R.A., Lyzenga, D.R., Rufenach, C.L., Tucker, M.J., 1985. Theory of synthetic aperture radar ocean imaging: A MARSEN view. J. Geophys. Res. 90, 4659. https://doi.org/10.1029/JC090iC03p04659

Johnsen, H., Collard, F., 2009. Sentinel-1 ocean swell wave spectra (osw) algorithm definition.

Kerbaol, V., Chapron, B., Vachon, P.W., 1998. Analysis of ERS-1/2 synthetic aperture radar wave mode imagettes. J. Geophys. Res. Ocean. 103, 7833–7846. https://doi.org/10.1029/97JC01579

Kohout, A.L., Williams, M.J.M., Toyota, T., Lieser, J., Hutchings, J., 2016. In situ observations of wave-induced sea ice breakup. Deep. Res. Part II Top. Stud. Oceanogr. 131, 22–27. https://doi.org/10.1016/j.dsr2.2015.06.010

Liu, A.K., Vachon, P.W., Peng, C.Y., 1991. Observation of wave refraction at an ice edge by Synthetic Aperture Radar. J. Geophys. Res. 96, 4803–4808. https://doi.org/10.1029/90JC02546

Lyzenga, D.R., Shuchman, R. a., Lyden, J.D., 1985. SAR Imaging of Waves in Water and Ice : Evidence for Velocity Bunching. J. Geophys. Res. 90, 1031–1036. https://doi.org/10.1029/JC090iC01p01031

Monteban, D., Lubbad, R., Pedersen, J.O.P., 2019. Use of satellite remote sensing to study wave-ice interactions in the marginal ice zone - A review, in: POAC Port and Ocean Engineering under Arctic Conditions. Delft.

Perrie, W., Hu, Y.C., 1997. Air-ice-ocean momentum exchange. Part II: Ice drift. J. Phys. Oceanogr. 27, 1976-1996--. https://doi.org/10.1175/1520-0485(1997)027<1976:AIOMEP>2.0.CO;2

Schulz-stellenfleth, J., Lehner, S., 2002. Spaceborne synthetic aperture radar observations of

ocean waves traveling into sea ice. Geophys. Res. Lett. 107, 1–19.
Shen, H., Perrie, W., Hu, Y., He, Y., 2018. Remote Sensing of Waves Propagating in the Marginal Ice Zone by SAR. J. Geophys. Res. Ocean. 123, 189–200. https://doi.org/10.1002/2017JC013148
Shuchman, R. a., Rufenach, C.L., Johannessen, O.M., 1994. Extraction of marginal ice zone thickness using gravity wave imagery. J. Geophys. Res. 99, 901. https://doi.org/10.1029/93JC01956
Squire, V.A., 2018. A fresh look at how ocean waves and sea ice interact. Philos. Trans. R. Soc. A Math. Phys. Eng. Sci. 376, 20170342. https://doi.org/10.1098/rsta.2017.0342
Squire, V.A., Duggan, J.P., Wadhams, P., Rottier, P.J., Liu, A.J., 1995. Of ocean waves and sea ice. Annu. Rev. Fluid Mech. 27, 115–168. https://doi.org/10.1146/annurev.fl.27.010195.000555
Stopa, J.E., Ardhuin, F., Thomson, J., Smith, M.M., Kohout, A., Doble, M., Wadhams, P., 2018. Wave Attenuation Through an Arctic Marginal Ice Zone on 12 October 2015. 1. Measurement of Wave Spectra and Ice Features From Sentinel 1A. J. Geophys. Res. Ocean. 123, 3619–3634. https://doi.org/10.1029/2018JC013791
Zhao, X., Shen, H.H., Cheng, S., 2015. Modeling ocean wave propagation under sea ice covers. Acta Mech. Sin. Xuebao 31, 1–15. https://doi.org/10.1007/s10409-015-0017-5